Report

Cell Reports

BRCA1 Accelerates CtIP-Mediated DNA-End Resection

Graphical Abstract

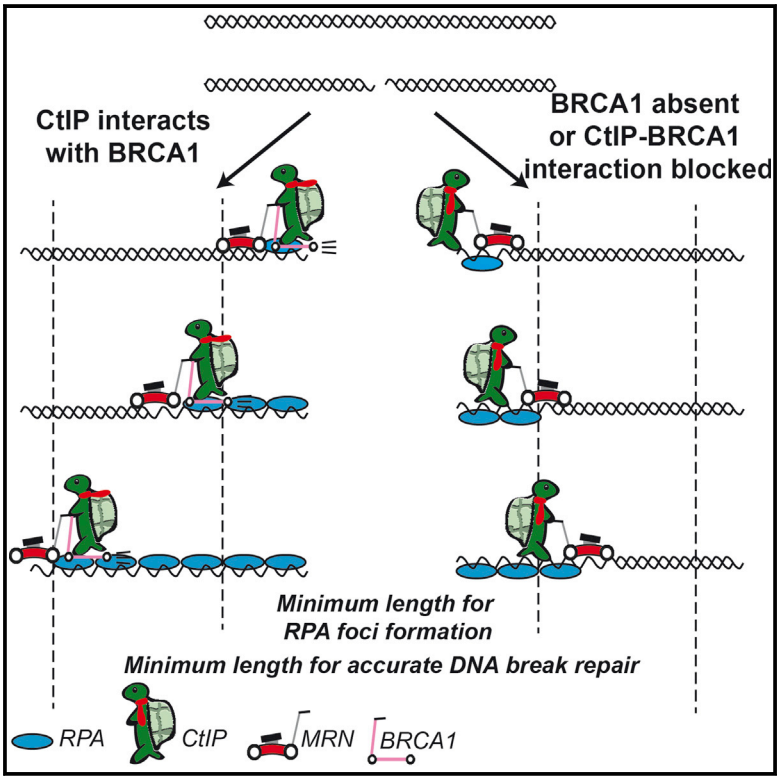

Highlights

A high-resolution method is used to measure DNA-end resection

BRCA1 interaction with CtIP is not essential for resection

BRCA1 interaction with CtIP affects resection speed

Authors

Andrés Cruz-García, Ana López-Saavedra, Pablo Huertas

Correspondence

pablo.huertas@cabimer.es

In Brief

CtIP is a key factor regulating DNA-end resection, an early step in DNA repair that controls the choice of repair pathway. CtIP interacts with BRCA1, but the exact role of BRCA1 in DNA-end resection is unclear. Cruz-García et al. develop a high-resolution method to measure the extent of DNA resection following DNA breaks. They find that resection occurs in the absence of a BRCA1-CtIP interaction, but the rate of resection is slower, suggesting that BRCA1 modulates its speed.

Cruz-García et al., 2014, Cell Reports 9, 451–459
October 23, 2014 ©2014 The Authors
http://dx.doi.org/10.1016/j.celrep.2014.08.076

Cell Reports
Report

BRCA1 Accelerates CtIP-Mediated DNA-End Resection

Andrés Cruz-García,[1,2] Ana López-Saavedra,[1,2] and Pablo Huertas[1,2,*]
[1]Centro Andaluz de Biología Molecular y Medicina Regenerativa (CABIMER), 41092 Sevilla, Spain
[2]Departamento de Genética, Universidad de Sevilla, 41080, Sevilla, Spain
*Correspondence: pablo.huertas@cabimer.es
http://dx.doi.org/10.1016/j.celrep.2014.08.076

SUMMARY

DNA-end resection is a highly regulated and critical step in the response and repair of DNA double-strand breaks. In higher eukaryotes, CtIP regulates resection by integrating cellular signals via its posttranslational modifications and protein-protein interactions, including cell-cycle-controlled interaction with BRCA1. The role of BRCA1 in DNA-end resection is not clear. Here, we develop an assay to study DNA resection in higher eukaryotes at high resolution. We demonstrate that the BRCA1-CtIP interaction, albeit not essential for resection, modulates the speed at which this process takes place.

INTRODUCTION

Repairing DNA double-strand breaks (DSBs) is essential to ensure cell and organismal survival (Aguilera and Gómez-González, 2008). In multicellular organisms, the complete absence of DSB repair produces severe phenotypes such as embryonic lethality, immune deficiency, and sterility (Aguilera and Gómez-González, 2008). While many different pathways contribute to repairing DSBs, these can be categorized into three groups according to their use of homology during the repair process (Huertas, 2010); use of long homologous sequences (homologous recombination [HR]), short homologous DNA tracks (microhomology-mediated end joining [MMEJ]), or no homology at all (nonhomologous end joining [NHEJ]). Coordinating all three pathways is extremely important for maintaining genome stability. The key event that controls the DSB repair pathway choice is DNA-end resection. This mechanism consists of a 5′ to 3′ degradation of one strand at each side of the break (Huertas, 2010). Since NHEJ is inhibited by DNA-end resection, the DNA end once resected is committed to being repaired by either HR or MMEJ (Huertas, 2010). In mammals, CtIP is so far the best known molecular switch that controls DNA-end resection and, therefore, DSB repair pathway choice (Escribano-Díaz et al., 2013; Huertas et al., 2008; Huertas and Jackson, 2009; Nakamura et al., 2010; Reczek et al., 2013; Sartori et al., 2007; Steger et al., 2013; Wang et al., 2013; Yun and Hiom, 2009). Among other modifications, CtIP is phosphorylated by cyclin-dependent kinases (CDKs) at many different residues, which serves to control its activity (Huertas et al., 2008; Huertas and Jackson, 2009), stability (Steger et al., 2013), or interaction with other factors (Nakamura et al., 2010; Reczek et al., 2013; Wang et al., 2013; Yun and Hiom, 2009). BRCA1, a tumor suppressor gene involved in recombination (Huen et al., 2010; Moynahan et al., 1999), interacts physically with CtIP in a CDK phosphorylation-mediated manner (Yu and Chen, 2004). Indirect evidences suggest that BRCA1-CtIP interaction plays a role in DSB repair pathway choice by affecting DNA-end resection, thereby facilitating the removal of the 53BP1-RIF1 complex (Cao et al., 2009; Chapman et al., 2013; Escribano-Díaz et al., 2013). Although one report claimed that CtIP mutants that block its interaction with BRCA1 in DT40 cells hamper DNA-end resection (Yun and Hiom, 2009), additional studies in DT40 and mice showed opposite results (Nakamura et al., 2010; Reczek et al., 2013).

Here we clarify the role of CtIP-BRCA1 interaction on DNA resection by different approaches. First, using CtIP mutants that change the interaction with BRCA1, we could demonstrate that such an interaction is involved in proper cell survival and checkpoint activation upon DNA damage. Second, we developed a technique that allows resection to be measured at high resolution in irradiation or drug-treated mammalian cells and to calculate resection speed. Using this technique, we observed that although resection could take place in the absence of an interaction between CtIP and BRCA1 it was slowed down. Thus, the CtIP-BRCA1 complex is not essential for DNA-end resection, but it modulates its speed.

RESULTS AND DISCUSSION

CtIP Mutants that Modify Its Interaction with BRCA1

The CtIP-BRCA1 interaction in human cells is controlled by the CDK-mediated phosphorylation of CtIP at serine 327 (S327) (Chen et al., 2008; Yu and Chen, 2004; Yu et al., 2006). Mutations that convert this serine to alanine abolish the interaction and render cells sensitive to different DNA-damaging agents (Chen et al., 2008; Nakamura et al., 2010; Reczek et al., 2013; Yu and Chen, 2004; Yu et al., 2006; Yun and Hiom, 2009). To study in more detail the role of the CtIP-BRCA1 complex on DNA-end resection and DNA repair, we used a green fluorescent protein (GFP)-tagged version of the CtIP-S327A mutant and a tagged-version of CtIP that constitutively interacts with BRCA1 by substituting S327 with aspartic acid, which mimics constitutive phosphorylation (CtIP-S327D allele; Figure 1A). First, we checked that the S327A and S327D mutants really modify the interaction with BRCA1. Indeed, the CtIP-S327A mutant blocked such an interaction, while the CtIP-S327D version reconstituted the interaction (Figure 1B). As the interaction of CtIP with BRCA1,

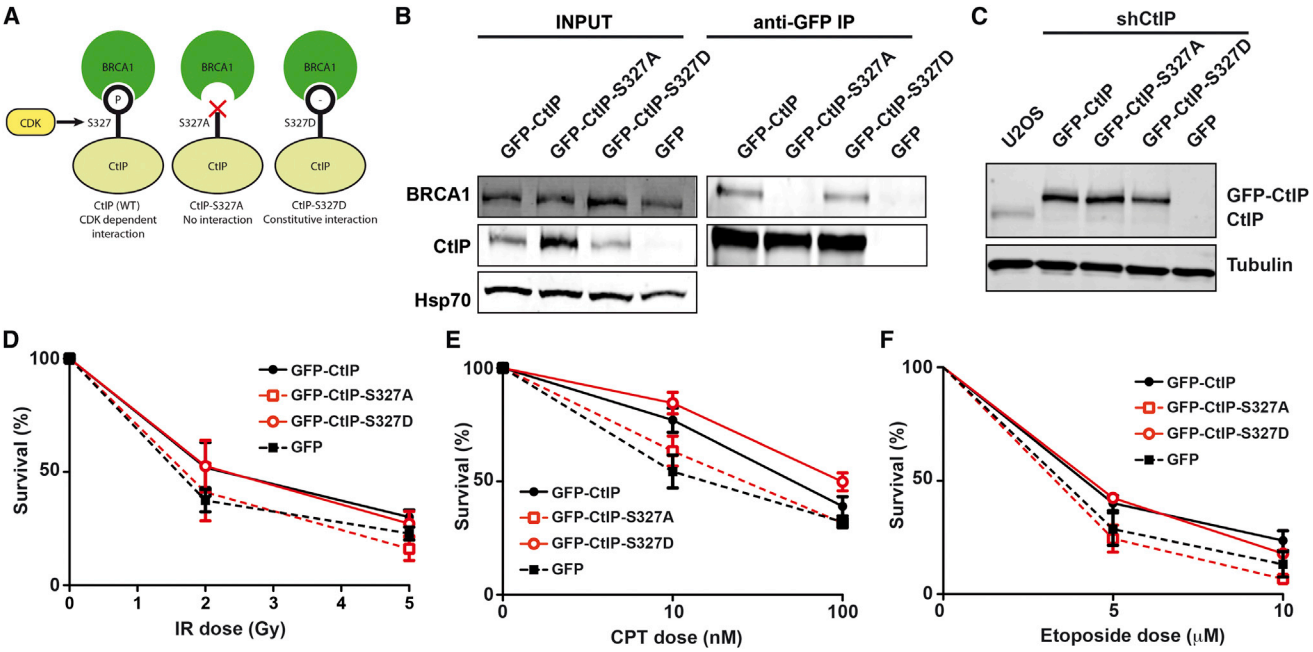

Figure 1. CtIP Mutations that Control Its Interaction with BRCA1

(A) Schematic representation of CtIP mutations and their effect on the interaction with BRCA1.

(B) Interaction of different CtIP mutants with BRCA1. GFP-CtIP and FLAG-BRCA1 were coimmunoprecipitated as described in the Experimental Procedures section. Protein samples were resolved in SDS-PAGE and blotted with the indicated antibodies.

(C) Expression of GFP-CtIP fusions upon downregulation of endogenous CtIP in U2OS cells. A sample from U2OS cells is shown for endogenous level of CtIP.

(D–F) Sensibility to IR (D), CPT (E), or ETOP (F) of U2OS cells harboring the indicated CtIP mutations. The mean and SD of three independent experiments are plotted.

See also Figure S1.

HR, and DNA-end resection are cell-cycle-regulated processes, we checked that not significant changes in cell-cycle distribution were observed in CtIP-S327A and CtIP-S327D backgrounds (Figure S1).

Blocking the CtIP-BRCA1 interaction render cells sensitive to several DNA-damaging agents, especially inhibitors of topoisomerases such as camptothecin (CPT) and etoposide (ETOP) (Chen et al., 2008; Nakamura et al., 2010; Reczek et al., 2013; Yu and Chen, 2004; Yu et al., 2006; Yun and Hiom, 2009). To confirm that this sensitivity is due to the lack of interaction, we performed clonogenic assays using U2OS cells stably transfected with different GFP-tagged versions of CtIP and depleted for endogenous CtIP (Figure 1C). We used ionizing radiation (IR) and ETOP, which damages the DNA in all phases of the cell cycle, and CPT, which only causes DSBs in the S phase coupled to replication. In agreement with previous results, CtIP-S327A mutants were as sensitive to IR, ETOP, and CPT as cells depleted for CtIP (Figures 1D–1F). Moreover, we conclude that the sensitivity to DNA damage is a direct consequence of the lack of interaction, as it was reverted to wild-type levels when CtIP constitutively interacts with BRCA1 (Figures 1D–1F).

CtIP and DNA Processing

Most reports on the CtIP-BRCA1 interaction agree that it is involved in DNA repair (Chen et al., 2008; Nakamura et al., 2010; Reczek et al., 2013; Yu and Chen, 2004; Yu et al., 2006; Yun and Hiom, 2009). However, it is less clear if this interaction is required for DNA-end resection (Nakamura et al., 2010; Reczek et al., 2013; Yun and Hiom, 2009).

Resected DNA is immediately coated by the single-stranded DNA (ssDNA)-protecting complex RPA. We first analyzed the appearance of RPA foci 1 hr after the DNA was challenged with a damaging agent of IR, CPT, or ETOP. Neither GFP-CtIP-S327A nor GFP-CtIP-S327D mutations had any apparent effect on RPA-foci formation after IR- or CPT-induced damage, in stark contrast with control cells expressing GFP (Figures 2A and 2B). Moreover, BRCA1 depletion also had little to no effect on RPA-foci formation (Figure 2A and B). Thus, we conclude that neither the BRCA1 nor the CtIP-BRCA1 interaction is essential for DNA-end resection on cells treated with IR or CPT. Coherent results were obtained when phosphorylation at serine 4 and serine 8 of RPA was used as a readout of DNA-end resection (Figure S2), but a mild not statistically significant reduction of phospho RPA was observed in CtIP-S327A after IR. However, a mild but clear decrease in RPA-foci was observed both in the CtIP-S327A and BRCA1 depletion when ETOP was used (Figure 2C). In agreement, the phospho RPA versus RPA ratio was decreased in CtIP-S327A to a similar extent as the GFP control (Figure S2). As ETOP traps topoisomerase II covalently bound to the 5′ end of the break, whereas CPT does the same to topoisomerase I at the 3′ end, we suspected that BRCA1 and the CtIP-BRCA1

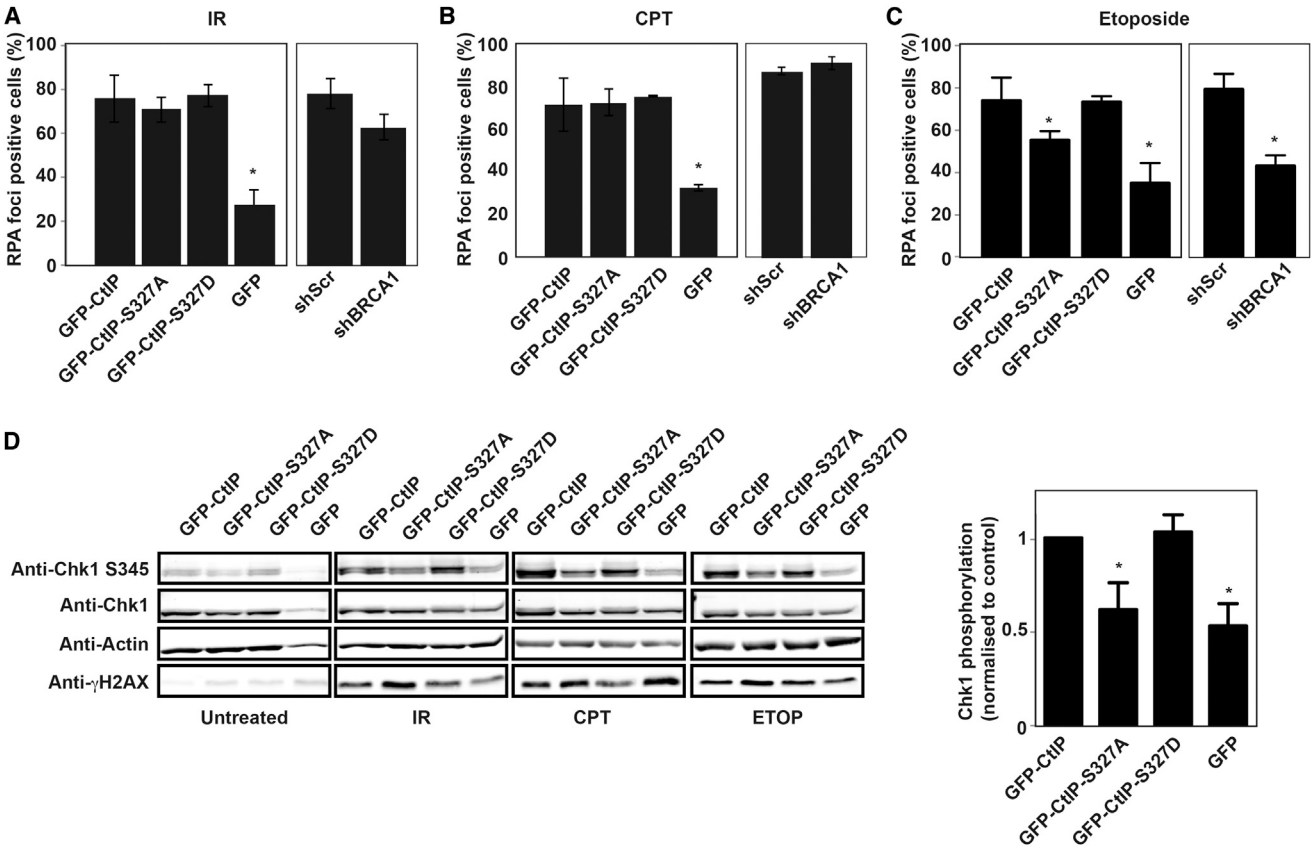

Figure 2. RPA Foci Formation in U2OS Cells Stably Transfected with CtIP S327 Mutants

(A–C) Percentage of γH2AX-positive cells with visible RPA-foci in different CtIP or BRCA1 background 1 hr after treatment with 10 Gy of IR (A), 1 μM of CPT (B), or 10 μM ETOP (C). The mean and SD of three independent experiments are plotted. Statistical significance was calculated as described in the Experimental Procedures section. See also Figure S2.

(D) ATR activity, as measured by Chk1 phosphorylation at S345, in cells harboring CtIP variants after the indicated genotoxic treatments. Protein samples were taken 1 hr after the treatment, collected as indicated in the Experimental Procedures section, and blotted with the indicated antibodies. A representative western blot (left) and quantification for Chk1 phosphorylation (right) are shown. Statistical significance was calculated as described in the Experimental Procedures section.

interaction are required to release proteins covalently bound to the 5′ end of the break. This situation resembles what happens during meiosis, in which the topoisomerase II-like enzyme Spo11 creates DSBs on the DNA (Neale et al., 2005). In budding yeast, drug-induced or IR-induced breaks are resected in the absence of the CtIP functional ortholog Sae2 due to the activity of exonucleases such as Exo1 (Moreau et al., 2001). However, the removal of Spo11 adducts in meiosis is completely dependent on Sae2 (Neale et al., 2005).

As an alternative readout for DNA-end processing, we decided to analyze the activation of the ATR branch of the DNA damage response. Resected DNA acts as a platform for the binding of the checkpoint complex ATRIP-ATR, which is essential for triggering the checkpoint (Zou and Elledge, 2003). In fact, the amount of ATRIP bound to DNA responds to the amount of RPA-coated ssDNA (Zou and Elledge, 2003). We then analyzed the activation of the ATR branch of the checkpoint by measuring the phosphorylation of Chk1 (Figure 2D). We observed that cells bearing the CtIP-S327A mutant, but not the CtIP-S327D, had a mild reduction in Chk1 activation, in agreement with a reduced length of resected ssDNA.

Based on these conflicting observations about the putative role of CtIP-BRCA1 interaction in DNA resection, we contemplated two alternative scenarios: either the CtIP-BRCA1 complex has a second role in DNA repair and ATR activation not related with resection or the lack of interaction between CtIP and BRCA1 has a role on DNA-end resection too subtle to be observed by RPA foci accumulation.

Single-Molecule Analysis of Resection Tracks

RPA-foci formation is a low-resolution technique to measure DNA-end resection that does not give information about the length of the resected DNA track (Figure 3A). In yeast, resection could be quantified at higher resolution (Clerici et al., 2006; Westmoreland et al., 2009; Zierhut and Diffley, 2008), but such approaches are difficult to apply in vertebrate cells. Only recently, a PCR-based assay has been developed for human cells; however, it is limited to the analysis of resection at sites created by

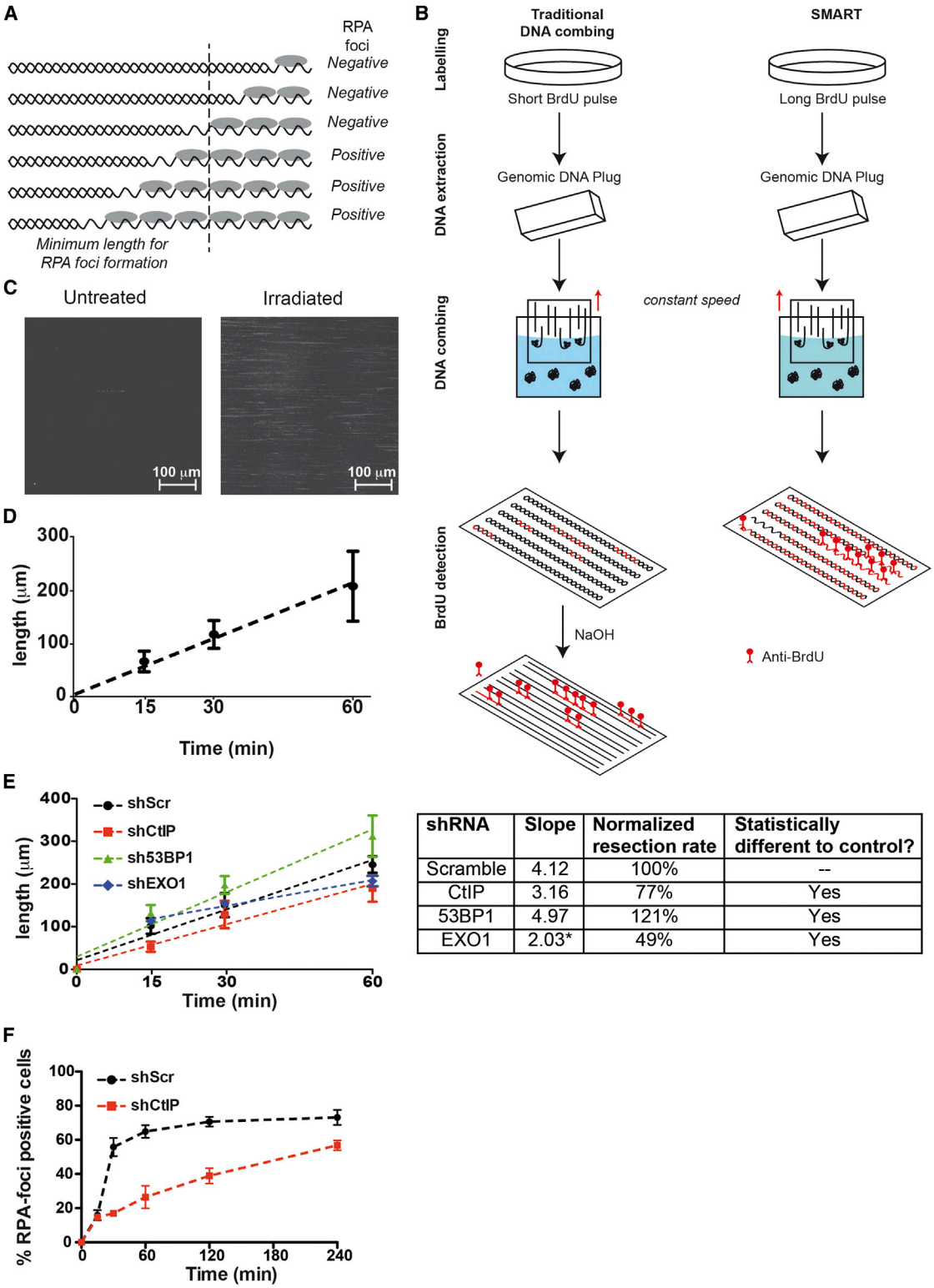

shRNA	Slope	Normalized resection rate	Statistically different to control?
Scramble	4.12	100%	--
CtIP	3.16	77%	Yes
53BP1	4.97	121%	Yes
EXO1	2.03*	49%	Yes

Figure 3. Single-Molecule Analysis of Resection Tracks

(A) Schematic representation of the limitation of RPA-foci scoring as a measurement of DNA-end resection. The two possible categories, e.g., RPA foci-positive or -negative cells, do not discriminate between resected DNA of different lengths.

(B) Graphic representation of the similarities and differences of the DNA combing (left) and the SMART (right) techniques to study replication or resection speed, respectively. In both cases, DNA was labeled with BrdU (indicated in red), isolated in plugs to minimize DNA shearing, stretched on a coverslip at constant speed,

(legend continued on next page)

endonucleases at specific sites of the genome (Zhou et al., 2014).

To analyze in more detail the putative role of CtIP-BRCA1 complex in resection, we have developed a technique for measuring the length of resected DNA at the level of single molecules: single-molecule analysis of resection tracks (SMARTs). This method can be easily extrapolated to any model cellular system from bacteria to human cells and can be used to analyze resection created by any damaging agent anywhere in the genome.

We based the SMART method on the DNA-combing technique (Herrick and Bensimon, 1999) (Figure 3B, left). This approach uses thymidine analogs, such as bromodeoxyuridine (BrdU), to determine the speed of replication. Briefly, a short pulse of a thymidine analog is followed by a gentle DNA purification. DNA molecules are stretched on a coverslip at a fixed speed, forming parallel fibers. Newly replicated DNA is then detected by immunofluorescence. However, anti-BrdU antibodies recognize an epitope that is usually hidden inside the DNA. Therefore, DNA has to be first denatured to expose the BrdU epitope, and then the coverslips are incubated with an anti-BrdU antibody. At the end, the newly synthesized DNA can be visualized as individual tracks, the length of which can be measured (Herrick and Bensimon, 1999).

BrdU has been previously used to study DNA resection at low resolution by cellular immunofluorescence (Raderschall et al., 1999). For this approach, a long BrdU pulse (20 to 24 hr) is required to allow one strand of every DNA molecule to be labeled. Upon DSB formation, DNA resection over BrdU-labeled DNA exposes the epitope recognized by the antibody and can readily be observed under the microscope without denaturation. This technique, similar as RPA-foci formation, is unable to measure how fast resection is taking place. We combined this approach with a modified DNA combing technique to visualize individual tracks of resected DNA (Figure 3B, right, SMART). Cells were exposed to BrdU for 24 hr, treated or mock treated with IR, and incubated 1 hr to allow DNA resection to take place. We isolated and stretched DNA and immunodetected BrdU in native conditions (Figure 3B, right). As observed in Figure 3C, almost no fibers were detected with the antibody from DNA from cells not treated with IR, indicating that the amount of ssDNA on unperturbed conditions is minimal. In contrast, irradiated samples showed multiple long tracks of BrdU-containing ssDNA. Extensive observation of several fields demonstrates that the number of fibers observed in untreated conditions was less than 1% of those visualized upon irradiation (Figure S3A). Moreover, those tracks observed in control cells were substantially shorter (Figure S3A). We reasoned that these short ssDNA tracks were either created during replication or reflect resection of endogenously aroused breaks. In contrast, irradiation creates abundant and long resection tracks. To validate the SMART technique, we made two predictions: first, if the ssDNAs are the product of an active process, such as DNA resection, they should grow at a specific rate, and second, ssDNAs should be affected by downregulation of proteins involved in the regulation and/or process of resection. To test the former idea, we performed the same experiment taking samples at several time points after irradiation from U2OS cells (Figure 3D). We measured the length of at least 200 single resection tracks at each time point per experiment. At each sample, we observed many different lengths of resected DNA (see Figure S3B and Table S1 for individual fibers quantification of representative experiments). We think this reflects different times of resection initiation, resection over different chromatin templates, etc. Similar heterogeneity of resection speed has been previously reported in budding yeast (Zierhut and Diffley, 2008). Thus, we calculate the medians of the measured resected tracks length at each time point as the representative value and then plot the average of the medians of three independent experiments. Strikingly, we observed that the lengths of those tracks grew following a straight line, suggesting a fixed speed of DNA resection. Moreover, a lack of CtIP not only reduced the number of fibers observed, but reduced DNA resection speed by 23% as compared with a control (Figure 3E). Thus, with the SMART technique, we can distinguish between two types of effects during resection: initiation and speed. Whereas the number of resection fibers will be an indication of resection initiation, the slope of the curve calculated with those breaks that are indeed resected will represent resection speed. Considering the physical characteristic of ssDNA on solution (Chi et al., 2013), we could estimate that the resection rate in the shRNA scramble control is about 0.2 kb/hr. This is 20 times slower than the resection calculated for HO breaks in budding yeast (Fishman-Lobell et al., 1992; Vaze et al., 2002). However, it has been shown that only 10% of the breaks actually reach such speed, but the majority is resected at a slower pace (Zierhut and Diffley, 2008). Indeed, such heterogeneity it is also observed with the SMART technique, as not all breaks are equally resected (Table S1). Moreover, in our case, the breaks are not the "clean" HO induced, but "ragged" IR created, which could also explain some of the difference.

We observed that CtIP depletion has a strong effect in resection initiation, as previously described, but also affects resection

and detected using an anti-BrdU antibody. Whereas a denaturation step (NaOH) is required to expose the BrdU epitope in the traditional combing technique, in the SMART technique resection directly exposes the epitope.

(C) A representative image of DNA fibers visualized with the anti-BrdU antibody with the SMART technology from cells untreated (left) or treated with 10 Gy of irradiation (right). See also Figure S3A.

(D) Representation of the mean of the medians of the length of 200 resected fibers at each time point in U2OS cells treated with shRNA control with their linear correlation (R^2 = 0.998). The mean and SDs of three independent experiments are plotted. See also Figure S3B.

(E) The same as in (D) but in cells expressing an shRNA against CtIP, 53BP1, EXO1 or a control shRNA (shScr). shCtIP: R^2 = 0.90. sh53BP1: R^2 = 0.92. shEXO1*: R^2 = 0.94. shScr: R^2 = 0.98. The absolute resection speed, calculated as the slope of the line, is indicated. The normalized resection rate, calculated normalizing the slope of each curve with the slope of shScr, is also shown. Statistical difference between slopes was calculated as described in the Methods section. *In the case of shEXO1 harboring cells, which followed a biphasic graph, the initial time point (0 min) was omitted for the linear regression. See also Figure S4.

(F) Percentage of γH2AX-positive cells with visible RPA-foci at different times after irradiation in cells transduced with shRNA against CtIP (shCtIP) or control (shScr). The mean and SD of four independent experiments are plotted.

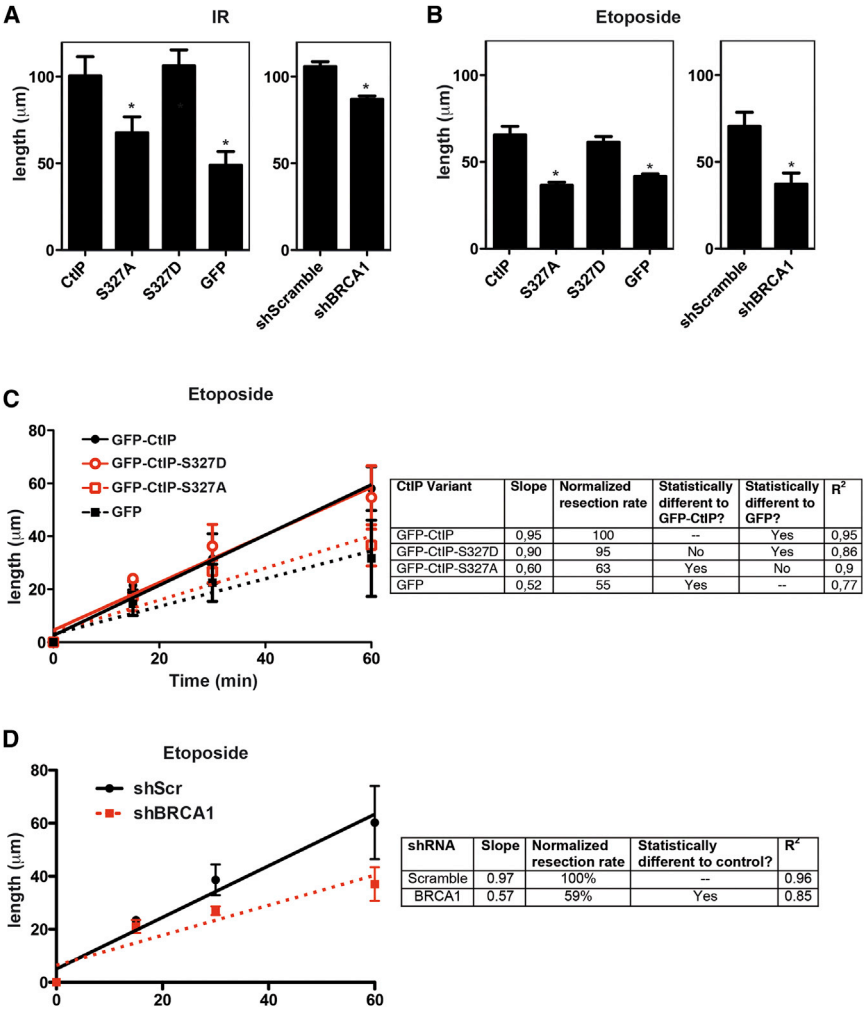

CtIP Variant	Slope	Normalized resection rate	Statistically different to GFP-CtIP?	Statistically different to GFP?	R^2
GFP-CtIP	0,95	100	--	Yes	0,95
GFP-CtIP-S327D	0,90	95	No	Yes	0,86
GFP-CtIP-S327A	0,60	63	Yes	No	0,9
GFP	0,52	55	Yes	--	0,77

shRNA	Slope	Normalized resection rate	Statistically different to control?	R^2
Scramble	0.97	100%	--	0.96
BRCA1	0.57	59%	Yes	0.85

Figure 4. The Interaction between CtIP and BRCA1 Accelerates DNA-End Resection

(A and B) SMART of U2OS cells harboring the indicated CtIP mutants or depleted for BRCA1 1 hr after IR (A) or ETOP (B) treatment. The mean and SDs of three independent experiments are shown. Statistical significance was calculated as described in the Experimental Procedures section.

(C) SMART was performed in U2OS cells expressing the indicated CtIP variants at different time points after addition of ETOP. The mean of three different experiments is plotted. Absolute (slope) and normalized resection rate, calculated as indicated in Figure 3E, are shown. The statistical difference of the slopes compared with either the GFP-CtIP or GFP cell lines was calculated as described in the Experimental Procedures section.

(D) Same as (B), but in cells depleted of BRCA1 and control cells.

speed. Surprisingly, the effect on resection speed was mild compared with the strong effect that CtIP depletion causes in RPA foci formation 1 hr after DNA damage (Huertas and Jackson, 2009; Sartori et al., 2007). One interpretation of this apparent contradiction is that in CtIP-depleted cells this mild resection speed defect is enough to shorten resected DNA tracks to avoid visualization of RPA foci by microscopy. We reasoned that, in that case, at later time points the number of cells with RPA foci in cells depleted of CtIP should approach normal levels. Indeed, when we analyzed the formation of RPA foci in control and CtIP-depleted cells at different time points, we realized that the large difference observed at early time points diminished with time, as the number of RPA foci-positive cells reach a plateau in control cells but keep increasing in shCtIP harboring cells. Thus, the SMART technique allowed us to visualize resection tracks in conditions in which RPA foci are not observed, i.e., 1 hr after DNA damage induction. The long-range resection machinery, i.e., EXO1 and BLM (Gravel et al., 2008; Huertas, 2010), might cause this resection observed in CtIP-depleted cells. This strongly resembles the data observed in budding yeast, in which in the absence of Sae2, Exo1 is able to resect the DNA, albeit at a slower pace (Clerici et al., 2006; Moreau et al., 2001).

In stark contrast, depletion of 53BP1 accelerates resection by over 20% (Figure 3E; see Figure S4 for depletion levels). This result agrees with the complex 53BP1-RIF1 blocking DNA-end resection (Cao et al., 2009; Chapman et al., 2013; Di Virgilio et al., 2013; Escribano-Díaz et al., 2013). Moreover, our results suggest that 53BP1, which is recruited to damaged chromatin in all cell-cycle phases and spreads over kilobases, not only impedes resection in G1 but in S and G2 also slows down resection. Interestingly, whereas the length of resected DNA in both CtIP and 53BP1 depletion fitted with a linear correlation, when we reduce the amount of EXO1, we observed a different picture. In this case, considering the whole kinetics, the linear correlation was poor (R^2 below 0.7). In fact, it seemed that the initial resection (up to 15 min) in EXO1-depleted cells was similar to control cells, but after that, point resection slows down to 50% (Figure 3E; see Figure S4 for depletion levels). Indeed, considering only time points between 15 and 120 min, the fitness to a linear correlation improved (R^2 = 0.94). This observation agrees with EXO1 being involved in a second phase of DNA-end resection and being dispensable for initiation (Gravel et al., 2008; Huertas, 2010).

Thus, we propose that this technique can be applied to measure the length of single-molecule resection tracks and to calculate resection rate. In contrast, RPA foci formation will reflect the contribution of a protein to both initiation and resection speed.

Resection Is Slower in CtIP-S327A Mutants

We used the SMART technique to analyze the speed of resection in different CtIP backgrounds (Figures 4A and 4B) after IR or ETOP treatment. First, we measured the length of resected

DNA in the same conditions we used to study RPA-foci formation, i.e., 1 hr following irradiation or the addition of the drug (Figures 2A and 2C). We observed that cells harboring CtIP-S327D resected as much as those bearing wild-type CtIP in both cases. In contrast, impairment of the CtIP-BRCA1 interaction (via the CtIP-S327A mutants) or BRCA1 depletion resulted in shorter resected tracks after both treatments. No difference was observed in the number of resected tracks, indicating that such an interaction is dispensable for resection initiation. Thus, we conclude that, although the CtIP-BRCA1 interaction is not essential for DNA-end resection (Figure 2), it affects the length of resected DNA. This could be explained by a reduction in resection speed, a delay in resection initiation, or an early stop in resection. This is especially important in ETOP-treated cells, in which the timing of topoisomerase II removal could influence the length of resected DNA. Therefore, we performed a kinetic study of resection in cells treated with ETOP (Figures 4C and 4D). We observed that resection speed is indeed reduced when CtIP cannot interact with BRCA1 or BRCA1 is absent to a similar extent as that observed in CtIP-depleted cells. In contrast, a constitutive interaction between CtIP and BRCA1 completely restored resection speed. Thus, we conclude that CtIP interaction with BRCA1 affects resection speed and that this effect is more prominent when the 5′ end of the DNA is blocked by a topoisomerase II-DNA adduct.

Considering all of our data collectively, we suggest that CtIP and the rest of the resection machinery are able to resect DNA breaks in the absence of BRCA1. However, BRCA1 action upon CtIP facilitates resection. This is likely due to the role that BRCA1 plays in removing RIF1-53BP1 complexes (Chapman et al., 2013; Escribano-Díaz et al., 2013). Indeed, CtIP-S327A mutants accumulate RIF1 foci in S and G2 phases of the cell cycle (Escribano-Díaz et al., 2013), and depletion of 53BP1 accelerates resection (Figure 3E). The subtle effects on DNA-end resection might explain some of the conflicting data in the literature based on RPA foci formation (Chapman et al., 2013; Escribano-Díaz et al., 2013; Nakamura et al., 2010; Reczek et al., 2013; Yun and Hiom, 2009). Resected DNA is essential for HR. However, long resected tracks are not required to engage the homologous sequence involved in this type of repair. That might explain why HR is not impaired in CtIP-S327A mutants (Nakamura et al., 2010). However, the length of resected DNA will impact checkpoint activation (Figure 2D) and will also affect the type of HR that will take place (Chandramouly et al., 2013; Huertas, 2010), thereby affecting in cell viability upon DNA damage induction. Thus, either the actual shortening of resected DNA or this mild checkpoint defect could account for the sensitivity to DNA-damaging agents observed in the CtIP-S327A mutant, although we cannot exclude an additional role for the CtIP-BRCA1 complex in DSB repair.

EXPERIMENTAL PROCEDURES

Cell Culture, Lentiviral Infection, and Cell Survival

U2OS or HEK293 cells stably expressing GFP-CtIP variants were grown in Dulbecco's modified Eagle's medium (Sigma-Aldrich) supplemented with 10% fetal bovine serum (Sigma-Aldrich), 100 units/ml penicillin, and 100 g/ml streptomycin (Sigma-Aldrich) supplemented with 0.5 mg/ml G418 (GIBCO). Lentiviral particles were obtained as previously described (Gomez-Cabello et al., 2013) using the plasmids listed in Table S2. Cell survival assays were performed as describe previously (Huertas and Jackson, 2009).

Immunofluorescence Microscopy

U2OS cells expressing GFP-CtIP fusions were infected with lentivirus harboring an shRNA targeted against CtIP. After 48 hr, cells were treated with 1 μM CPT, 10 μM ETOP, 10 Gy of IR, or mock treated, incubated 1 hr for foci formation, and then collected. Coverslips were treated for 5 min on ice with pre-extraction buffer (25 mM HEPES [pH 7.4], 50 mM NaCl, 1 mM EDTA, 3 mM $MgCl_2$, 300 mM sucrose, and 0.5% Triton X-100) and then fixed with 2% paraformaldehyde (w/v) in PBS for 15 min, washed three times with PBS, and blocked for at least 1 hr with 5% fetal bovine serum (FBS) diluted in PBS. Cells were incubated with the adequate primary antibodies (Table S3), diluted in 5% FBS in PBS for 2 hr at room temperature, washed with PBS, and then incubated with secondary antibodies (Table S4) diluted in 5% FBS in PBS for 1 hr at room temperature. Cells were then washed twice with PBS, and coverslips were mounted with Vectashield mounting medium (Vector Laboratories) containing 4′,6-diamidino-2-phenylindole and analyzed using a Nikon NI-E microscope.

Immunoblotting

Extracts were prepared in Laemmli buffer (4% SDS, 20% glycerol, 120 mM Tris-HCl [pH 6.8]), and proteins were resolved by SDS-PAGE and transferred to polyvinylidene fluoride (Millipore) followed by immunoblotting. Western blot analysis was carried out using the antibodies listed in Tables S3 and S4. Results were visualized using an Odyssey Infrared Imaging System (Li-Cor). To quantify Chk1 phosphorylation, protein abundance was measured using the Li-Cor software, and the ratio between phosphorylated Chk1 and total Chk1 was calculated. Those ratios were then normalized with respect to control cells expressing full-length CtIP.

Immunoprecipitation

HEK293T cells stably expressing GFP-CtIP variants were cotransfected with HALO-BARD1 and SFB-BRCA1 expression vectors (a gift from Ko Sato, St. Marianna University Graduate School of Medicine) and shCtIP (Sigma-Aldrich). At 48 hr after transfection, cells were harvested in a lysis buffer of 50 mM Tris-HCl [pH 7.4], 100 mM NaCl, 1 mM EDTA, 0.2% de Triton X-100, 1× protease inhibitors (Escribano-Díaz et al., 2013), 1× phosphatase inhibitor cocktail 1 (Sigma). Protein extract (1 mg) was incubated with 20 μl of packed anti-GFP_ M magnetic beads (Chromotek) at 4°C. Beads were then washed three times with lysis buffer, and precipitate was eluted in Laemmli buffer.

SMART

U2OS cells, either wild-type or stably expressing GFP-CtIP variants or depleted of the indicated proteins, were grown in the presence of 10 μM BrdU (GE Healthcare) for 24 hr. Cultures were then irradiated (10 Gy) and harvested at the indicated time points. DNA combing was performed as previously described with modifications (Michalet et al., 1997). Briefly, cells were embedded in low-melting agarose (Bio-Rad) followed by DNA extraction. To stretch the DNA fibers, silanized coverslips (Genomic Vision) were dipped into the DNA solution for 15 min and pulled out a constant speed (250 μm/s). Coverslips were baked for 2 hr at 60°C and incubated directly without denaturation with an anti-BrdU mouse monoclonal (Table S3). After washing with PBS, coverslips were incubated with the secondary antibody (Table S4). Finally, coverslips were mounted with ProLong Gold Antifade Reagent (Molecular Probes) and stored at −20°C. DNA fibers were observed with Nikon NI-E microscope and PLAN FLOUR40 ×/0.75 PHL DLL objective. The images were recorded and processed with NIS ELEMENTS Nikon software. For each experiment, a total of 200 DNA fibers was analyzed, and the length of DNA fibers was measured with Adobe Photoshop CS4 Extended version 11.0 (Adobe Systems).

For resection speed, SMART results at different time points were plotted. After doing a linear correlation, the resection rate was calculated as the slope of the line. To compare between treatments, slopes were normalized with respect to control cells expressing full-length CtIP.

Statistical Analysis

Statistical significance was determined with a paired t student test using the PRISM software (Graphpad Software) for all data sets, with the exception of

the slope comparison shown in Figures 3E, 4C, and 4D. In that particular case, the slope comparison was performed as described in Chapter 18 of *Biostatistical Analysis* (Zar, 1984).

SUPPLEMENTAL INFORMATION

Supplemental Information includes four figures and four tables and can be found with this article online at http://dx.doi.org/10.1016/j.celrep.2014.08.076.

AUTHOR CONTRIBUTIONS

A.C.-G. performed all of the experiments described. A.L.-S. helped with the analysis by SMART of BRCA1 depletion. The project and SMART method were conceived, designed, and developed by P.H. with the help of A.C.-G. All authors contributed to the discussion of the results. P.H. wrote the paper with the feedback of A.C.-G.

ACKNOWLEDGMENTS

We thank Sonia Barroso and Andrés Aguilera for technical advice, Ko Sato for sharing reagents, Veronica Raker for style corrections, and Felix Prado, Sonia Jimeno, and Cristina Cepeda for critical reading of the manuscript. This work was funded by an R+D+I grant from the Spanish Ministry of Economy and Competitivity (SAF2010-14877). A.C.-G. is funded by a PhD fellowship from the Consejo Nacional de Ciencia y Tecnología (CONACYT). A.L.-S. is the recipient of a predoctoral training fellowship from the Spanish Ministry of Science and Innovation (FPI fellowship).

Received: March 18, 2014
Revised: July 10, 2014
Accepted: August 27, 2014
Published: October 9, 2014

REFERENCES

Aguilera, A., and Gómez-González, B. (2008). Genome instability: a mechanistic view of its causes and consequences. Nat. Rev. Genet. *9*, 204–217.

Cao, L., Xu, X., Bunting, S.F., Liu, J., Wang, R.H., Cao, L.L., Wu, J.J., Peng, T.N., Chen, J., Nussenzweig, A., et al. (2009). A selective requirement for 53BP1 in the biological response to genomic instability induced by Brca1 deficiency. Mol. Cell *35*, 534–541.

Chandramouly, G., Kwok, A., Huang, B., Willis, N.A., Xie, A., and Scully, R. (2013). BRCA1 and CtIP suppress long-tract gene conversion between sister chromatids. Nat Commun *4*, 2404.

Chapman, J.R., Barral, P., Vannier, J.B., Borel, V., Steger, M., Tomas-Loba, A., Sartori, A.A., Adams, I.R., Batista, F.D., and Boulton, S.J. (2013). RIF1 is essential for 53BP1-dependent nonhomologous end joining and suppression of DNA double-strand break resection. Mol. Cell *49*, 858–871.

Chen, L., Nievera, C.J., Lee, A.Y., and Wu, X. (2008). Cell cycle-dependent complex formation of BRCA1.CtIP.MRN is important for DNA double-strand break repair. J. Biol. Chem. *283*, 7713–7720.

Chi, Q., Wang, G., and Jiang, J. (2013). The persistence length and length per base of single-stranded DNA obtained from fluorescence correlation spectroscopy measurements using mean field theory. Physica A *392*, 1072–1079.

Clerici, M., Mantiero, D., Lucchini, G., and Longhese, M.P. (2006). The Saccharomyces cerevisiae Sae2 protein negatively regulates DNA damage checkpoint signalling. EMBO Rep. *7*, 212–218.

Di Virgilio, M., Callen, E., Yamane, A., Zhang, W., Jankovic, M., Gitlin, A.D., Feldhahn, N., Resch, W., Oliveira, T.Y., Chait, B.T., et al. (2013). Rif1 prevents resection of DNA breaks and promotes immunoglobulin class switching. Science *339*, 711–715.

Escribano-Díaz, C., Orthwein, A., Fradet-Turcotte, A., Xing, M., Young, J.T., Tkáč, J., Cook, M.A., Rosebrock, A.P., Munro, M., Canny, M.D., et al. (2013). A cell cycle-dependent regulatory circuit composed of 53BP1-RIF1 and BRCA1-CtIP controls DNA repair pathway choice. Mol. Cell *49*, 872–883.

Fishman-Lobell, J., Rudin, N., and Haber, J.E. (1992). Two alternative pathways of double-strand break repair that are kinetically separable and independently modulated. Mol. Cell. Biol. *12*, 1292–1303.

Gomez-Cabello, D., Jimeno, S., Fernández-Ávila, M.J., and Huertas, P. (2013). New tools to study DNA double-strand break repair pathway choice. PLoS ONE *8*, e77206.

Gravel, S., Chapman, J.R., Magill, C., and Jackson, S.P. (2008). DNA helicases Sgs1 and BLM promote DNA double-strand break resection. Genes Dev. *22*, 2767–2772.

Herrick, J., and Bensimon, A. (1999). Single molecule analysis of DNA replication. Biochimie *81*, 859–871.

Huen, M.S., Sy, S.M., and Chen, J. (2010). BRCA1 and its toolbox for the maintenance of genome integrity. Nat. Rev. Mol. Cell Biol. *11*, 138–148.

Huertas, P. (2010). DNA resection in eukaryotes: deciding how to fix the break. Nat. Struct. Mol. Biol. *17*, 11–16.

Huertas, P., and Jackson, S.P. (2009). Human CtIP mediates cell cycle control of DNA end resection and double strand break repair. J. Biol. Chem. *284*, 9558–9565.

Huertas, P., Cortés-Ledesma, F., Sartori, A.A., Aguilera, A., and Jackson, S.P. (2008). CDK targets Sae2 to control DNA-end resection and homologous recombination. Nature *455*, 689–692.

Michalet, X., Ekong, R., Fougerousse, F., Rousseaux, S., Schurra, C., Hornigold, N., van Slegtenhorst, M., Wolfe, J., Povey, S., Beckmann, J.S., and Bensimon, A. (1997). Dynamic molecular combing: stretching the whole human genome for high-resolution studies. Science *277*, 1518–1523.

Moreau, S., Morgan, E.A., and Symington, L.S. (2001). Overlapping functions of the Saccharomyces cerevisiae Mre11, Exo1 and Rad27 nucleases in DNA metabolism. Genetics *159*, 1423–1433.

Moynahan, M.E., Chiu, J.W., Koller, B.H., and Jasin, M. (1999). Brca1 controls homology-directed DNA repair. Mol. Cell *4*, 511–518.

Nakamura, K., Kogame, T., Oshiumi, H., Shinohara, A., Sumitomo, Y., Agama, K., Pommier, Y., Tsutsui, K.M., Tsutsui, K., Hartsuiker, E., et al. (2010). Collaborative action of Brca1 and CtIP in elimination of covalent modifications from double-strand breaks to facilitate subsequent break repair. PLoS Genet. *6*, e1000828.

Neale, M.J., Pan, J., and Keeney, S. (2005). Endonucleolytic processing of covalent protein-linked DNA double-strand breaks. Nature *436*, 1053–1057.

Raderschall, E., Golub, E.I., and Haaf, T. (1999). Nuclear foci of mammalian recombination proteins are located at single-stranded DNA regions formed after DNA damage. Proc. Natl. Acad. Sci. USA *96*, 1921–1926.

Reczek, C.R., Szabolcs, M., Stark, J.M., Ludwig, T., and Baer, R. (2013). The interaction between CtIP and BRCA1 is not essential for resection-mediated DNA repair or tumor suppression. J. Cell Biol. *201*, 693–707.

Sartori, A.A., Lukas, C., Coates, J., Mistrik, M., Fu, S., Bartek, J., Baer, R., Lukas, J., and Jackson, S.P. (2007). Human CtIP promotes DNA end resection. Nature *450*, 509–514.

Steger, M., Murina, O., Hühn, D., Ferretti, L.P., Walser, R., Hänggi, K., Lafranchi, L., Neugebauer, C., Paliwal, S., Janscak, P., et al. (2013). Prolyl isomerase PIN1 regulates DNA double-strand break repair by counteracting DNA end resection. Mol. Cell *50*, 333–343.

Vaze, M.B., Pellicioli, A., Lee, S.E., Ira, G., Liberi, G., Arbel-Eden, A., Foiani, M., and Haber, J.E. (2002). Recovery from checkpoint-mediated arrest after repair of a double-strand break requires Srs2 helicase. Mol. Cell *10*, 373–385.

Wang, H., Shi, L.Z., Wong, C.C., Han, X., Hwang, P.Y., Truong, L.N., Zhu, Q., Shao, Z., Chen, D.J., Berns, M.W., et al. (2013). The interaction of CtIP and Nbs1 connects CDK and ATM to regulate HR-mediated double-strand break repair. PLoS Genet. *9*, e1003277.

Westmoreland, J., Ma, W., Yan, Y., Van Hulle, K., Malkova, A., and Resnick, M.A. (2009). RAD50 is required for efficient initiation of resection and recombinational repair at random, gamma-induced double-strand break ends. PLoS Genet. *5*, e1000656.

Yu, X., and Chen, J. (2004). DNA damage-induced cell cycle checkpoint control requires CtIP, a phosphorylation-dependent binding partner of BRCA1 C-terminal domains. Mol. Cell. Biol. *24*, 9478–9486.

Yu, X., Fu, S., Lai, M., Baer, R., and Chen, J. (2006). BRCA1 ubiquitinates its phosphorylation-dependent binding partner CtIP. Genes Dev. *20*, 1721–1726.

Yun, M.H., and Hiom, K. (2009). CtIP-BRCA1 modulates the choice of DNA double-strand-break repair pathway throughout the cell cycle. Nature *459*, 460–463.

Zar, J.H. (1984). Biostatistical Analysis, Second Edition (Englewood Cliffs, New Jersey: Prentice-Hall).

Zhou, Y., Caron, P., Legube, G., and Paull, T.T. (2014). Quantitation of DNA double-strand break resection intermediates in human cells. Nucleic Acids Res. *42*, e19.

Zierhut, C., and Diffley, J.F. (2008). Break dosage, cell cycle stage and DNA replication influence DNA double strand break response. EMBO J. *27*, 1875–1885.

Zou, L., and Elledge, S.J. (2003). Sensing DNA damage through ATRIP recognition of RPA-ssDNA complexes. Science *300*, 1542–1548.